IEEE Access
Multidisciplinary | Rapid Review | Open Access Journal

Received 31 December 2023, accepted 30 January 2024, date of publication 7 February 2024, date of current version 21 February 2024.

Digital Object Identifier 10.1109/ACCESS.2024.3364101

RESEARCH ARTICLE

Combined Observer and Lyapunov-Based Control for Switching Power Converters With LC Input Filter

ROGHAYEH GAVAGSAZ-GHOACHANI[1], MATHEEPOT PHATTANASAK[2], (Senior Member, IEEE), EHSAN JAMSHIDPOUR[3], (Senior Member, IEEE), WISET SAKSIRI[2], AND SERGE PIERFEDERICI[4]

[1]Mechanical and Energy Engineering, Department of Renewable Energies, Shahid Beheshti University, Tehran 1983969411, Iran
[2]Department of Teacher Training in Electrical Engineering, King Mongkut's University of Technology North Bangkok, Bangkok 10800, Thailand
[3]GREEN, University of Lorraine, 54000 Nancy, France
[4]LEMTA, University of Lorraine, 54000 Nancy, France

Corresponding author: Wiset Saksiri (wiset@kmutnb.ac.th)

This work was supported in part by the International Research Partnership "Electrical Engineering–Thai French Research Center" under the Project Framework of Lorraine Université d'Excellence in cooperation between Université de Lorraine and King Mongkut's University of Technology North Bangkok. This research was funded by the King Mongkut's University of Technology North Bangkok under Grant KMUTNB-66-KNOW-10.

ABSTRACT This paper presents a control technique for a boost converter that is connected to a power source via an LC input filter in a continuous conduction mode. The proposed method employs the Lyapunov stability criterion to determine the switching command that guarantees system stability. An estimator is introduced to track the load resistance and losses of the system in real-time. Our control strategy regulates all state variables of the system and additional state variables in the estimator concurrently. Additionally, the start-up transient response is considered in the control algorithm. Finally, experimental results are provided to validate the effectiveness of the proposed control method.

INDEX TERMS Boost converter, continue conduction mode, LC filter, stability, Lyapunov criterion.

I. INTRODUCTION

Power electronic converters are commonly used in various applications, including renewable energy [1], [2], [3], [4], [5], microgrids [6] and transportation [7], [8], [9], [10]. To minimize current and voltage ripples in the DC grid, an LC filter is typically placed at the input of the switching converter, as shown in Fig. 1. However, in the early 1970s, it was discovered that an incremental resistance at the input of the converter could be negative and interact with the LC filter, leading to instability [11]. A method was proposed to prevent this oscillation, and a guideline for designing the LC input filter was published to avoid unstable operation in the DC grid [12]. Negative resistance in tightly controlled power switching converters can be considered a constant power load (CPL) if the input current decreases to maintain constant input power as the input voltage increases [13]. As a result, the input resistance is negative. CPLs are common in transportation systems where DC microgrids power tightly controlled converter-driven motors [14], [15]. Researchers have developed various techniques to control CPLs and prevent unstable operations.

In the literature, researchers have primarily focused on four categories of research related to stability and instability zones in switching converters. The first category is focused on finding these zones to restrict the operation point of the switching converters [15]. The second category aims to increase the damping factor of the LC input filter using passive elements [16] or a passive stabilizer, which can lead to a low-efficiency system. The third category involves introducing special terms in the control algorithm, known as an active stabilizer, to provide a larger stability

The associate editor coordinating the review of this manuscript and approving it for publication was Snehal Gawande.

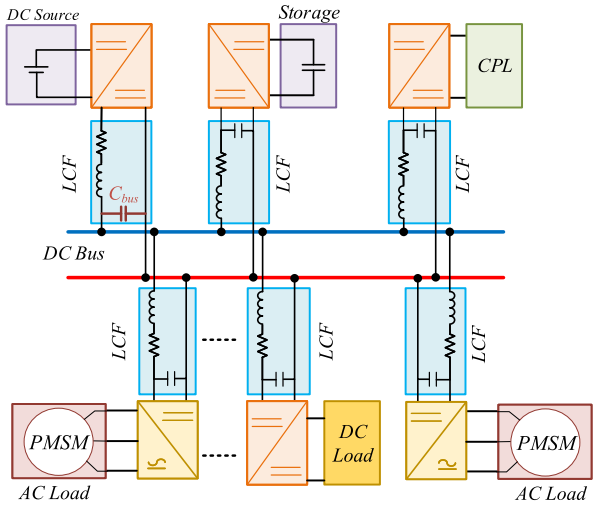

FIGURE 1. Example of a DC microgrid system with several loads including CPLs.

operation zone [17], [18], [19], [20], [21], [22]. This method typically mimics passive stabilizers, such as virtual impedance [26], [27] and virtual capacitors [17]. The final category focuses on controlling all state variables of the system, including those of the LC filter and switching converters.

Classically, to control a switching converter, the two-loop cascade feedback control method with pulse-width modulation (PWM) is commonly used [18]. The voltage outer-loop bandwidth must be lower than that of the current inner loop. The active stabilizer may be added to the control loop in several manners, e.g., at the outer loop [22], current inner loop [20], [21], [22], [23], [24], [25], and duty cycle [18], [19], [21]. In [26], the authors proposed a control strategy using the state feedback and pole placement to stabilize PWM DC-DC buck converters with input filters. To use this method, a linearized model was first developed. Therefore, the limitation of this control depends on the validity of that linearized model. In [27], the authors proposed a method to control all state variables that were inspired by [28], [29], and [30] using a switched model without linearization. However, because the control requires an exact value of components including the load, steady-state errors occur, particularly on the output voltage, which is one of the most important objectives. Moreover, the sampling frequency affects the steady-state error, as detailed in [31]. A higher sampling frequency makes the system operate with less steady-state error. However, a high-performance controller is required. Parts of the uncertainties of the system are present in the losses in the system, which depend on the operating point. If these losses are known, the controller can effectively compensate the losses, and the output voltage static error is consequently eliminated. Unknown parameters such as the capacitance, inductance, or losses in the switching power converters can be estimated using an estimator [32], [33]. Another drawback of the proposed control in [27] is the matrix P, which is the solution of the Lyapunov function depending on the operating point. When the operating point of this controlled system changes, the matrix P must be changed to stabilize the system. Therefore, P must be either calculated online or pre-calculated offline and put in a lookup table.

In contrast to [34], there are several significant differences in the underlying concept of the proposed control scheme. First, the control scheme provides guidelines for the startup, calculation of matrix P in detail, and modification of the control block diagram. Additionally, simulation results for the startup response, steady-state response, and transient response are presented. Furthermore, the experimental setup is described in detail, and more experimental results are included.

This paper presents an estimator that can estimate losses and load resistance, thereby reducing errors associated with these factors. Furthermore, the need for a current sensor to measure the output current is eliminated by embedding an observer based on Lyapunov stability criteria into the controller algorithm. Additionally, a start-up process method is proposed, and linear matrix inequalities (LMI) are utilized to reduce the matrix P to a single value.

This paper is organized as follows. Section II of the article describes the model of the boost converter with the LC input filter and the observer used in the study. In Section III, simulation results are presented to verify the effectiveness of the observer and controller. These results are then experimentally validated in Section IV.

II. SYSTEM DESCRIPTION AND LOSS MODEL

The system shown in Fig. 2 is comprised of an LC input filter (L_f, C_f), a boost converter with a switching command u∈{0,1}, an inductor L, an output capacitor C, and a resistive load R. The considered model accounts only for the parasitic resistances of the filter and converter inductors, denoted as r_f and r, respectively.

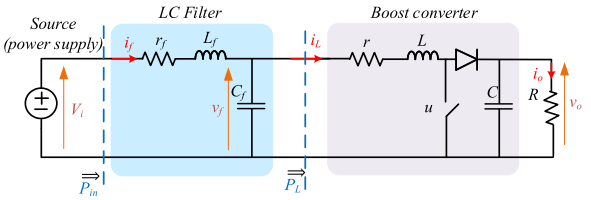

FIGURE 2. Example system: the power source is connected to a boost converter through an LC filter.

In Fig. 3, an ideal converter is considered, and losses are represented by a series independent voltage source V_T and a parallel independent current source I_P, inspired by [33]. V_T represents losses that depend on the level of input current, while I_P represents losses due to the output voltage.

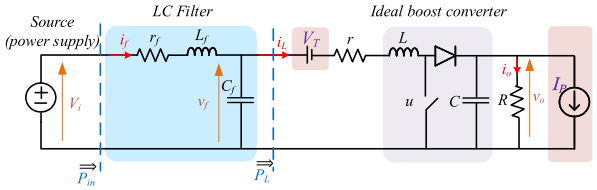

FIGURE 3. Studied system that represents losses by voltage V_T and current I_P.

The differential equations governing the behavior of the studied boost converter, connected to the power supply V_i, are given by:

$$\begin{cases} \dfrac{di_L}{dt} = \dfrac{1}{L}(v_f - V_T - ri_L - (1-u)v_o) \\ \dfrac{dv_o}{dt} = \dfrac{1}{C}((1-u)i_L - \dfrac{v_o}{R} - I_P) \end{cases} \tag{1}$$

The behavior of the LC input filter is described by the following differential equations:

$$\begin{cases} \dfrac{di_f}{dt} = \dfrac{1}{L_f}(V_i - r_f i_f - v_f) \\ \dfrac{dv_f}{dt} = \dfrac{1}{C_f}(i_f - i_L) \end{cases} \tag{2}$$

The control method proposed in [27] involves defining the switching command for the boost converter, u, to ensure the stability of the entire system at each sampling time, $T_s = \frac{1}{f_s}$, where f_s is the sampling frequency. The first step is to select a Lyapunov function candidate, followed by evaluating the time derivative of the Lyapunov function candidate to determine when to turn on and off the switch. The switching command that stabilizes the system is then selected. This method guarantees the global stability of the system during operation.

A. CONTROLLER

Considering Fig. 3, one can express the following equation depending on the switching command $u \in \{0, 1\}$ as:

$$\begin{cases} \dot{x} = A(u)x + B(u) - g(u) \cdot p \\ with \\ A(u) = A_1 u + A_2(1-u) \\ B(u) = B_1 u + B_2(1-u) \end{cases} \tag{3}$$

The considered system is described by state variables $x \in \Re^n$, $n = 4$, $x = \begin{bmatrix} i_f & v_f & i_L & v_o \end{bmatrix}^T$. Here, i_f represents the input current, v_f represents the filter capacitor voltage, i_L represents the boost inductor current, and v_o represents the output voltage. The system is powered by input voltage V_i. When the switching command $u = 1$, the system is described by matrices $A_1 \in \Re^{n\times n}$, $B_1 \in \Re^n$ as follows (equation (4)),

$$\dot{x} = A_1 x + B_1 - g \cdot p \tag{4}$$

with

$$A_1 = \begin{bmatrix} -\frac{r_f}{L_f} & -\frac{1}{L_f} & 0 & 0 \\ \frac{1}{C_f} & 0 & -\frac{1}{C_f} & 0 \\ 0 & \frac{1}{L} & -\frac{r}{L} & -\frac{1}{L} \\ 0 & 0 & 0 & -\frac{1}{RC} \end{bmatrix}, B_1 = \begin{bmatrix} \frac{V_i}{L_f} \\ 0 \\ 0 \\ 0 \end{bmatrix}$$

$$g = \begin{bmatrix} 0 & 0 \\ 0 & 0 \\ \frac{1}{L} & 0 \\ 0 & \frac{1}{C} \end{bmatrix}, p = \begin{bmatrix} V_T \\ I_P \end{bmatrix}$$

When $u = 0$, the system is described by matrices $A_2 \in \Re^{n\times n}$, $B_2 \in \Re^n$. The matrix $g \in \Re^{n\times m}$, where $m = 2$, and $p \in \Re^m$ represents the vector of voltage V_T and current I_P. Further details regarding these matrices are provided below:

$$\dot{x} = A_2 x + B_2 - g \cdot p \tag{5}$$

with

$$A_2 = \begin{bmatrix} -\frac{r_f}{L_f} & -\frac{1}{L_f} & 0 & 0 \\ \frac{1}{C_f} & 0 & -\frac{1}{C_f} & 0 \\ 0 & \frac{1}{L} & -\frac{r}{L} & -\frac{1}{L} \\ 0 & 0 & \frac{1}{C} & -\frac{1}{RC} \end{bmatrix}, B_1 = \begin{bmatrix} \frac{V_i}{L_f} \\ 0 \\ 0 \\ 0 \end{bmatrix}$$

$$g = \begin{bmatrix} 0 & 0 \\ 0 & 0 \\ \frac{1}{L} & 0 \\ 0 & \frac{1}{C} \end{bmatrix}, p = \begin{bmatrix} V_T \\ I_P \end{bmatrix}$$

When the converter operates at the equilibrium point where $x = x_{ref}$, assuming that the estimated value of p, denoted as $\hat{p} \in \Re^m$, where $m = 2$, $\hat{p} = \begin{bmatrix} \widehat{V_T} & \widehat{I_P} \end{bmatrix}^T$, is known, it can be verified that:

$$\dot{x}_{ref} = A(u_{ref})x_{ref} + B(u_{ref}) - g \cdot \hat{p} \tag{6}$$

with

$$A(u_{ref}) = u_{ref}A_1 + (1-u_{ref})A_2 \tag{7}$$

$$B(u_{ref}) = u_{ref}B_1 + (1-u_{ref})B_2 \tag{8}$$

Now, for simplicity, we introduce a new state variable z. Then, we can define the corresponding variable of z : $\hat{z}$ represents an estimated value of z, and $\dot{z}$ is the time derivative of z:

$$\begin{cases} z = x - x_{ref} \\ \hat{z} = \hat{x} - x_{ref} \\ \dot{z} = \dot{x} - \dot{x}_{ref} \end{cases} \tag{9}$$

Using (3) and (9), one can find the following expression:

$$\dot{z} = [A(u)z + A(u)x_{ref} + B(u) - A(u_{ref})x_{ref} - B(u_{ref})] - g(p - \hat{p}) - \dot{x}_{ref} \tag{10}$$

Noted, 10 implies that the time derivative of x_{ref}, denoted by $\dot{x}_{ref}$, is zero when the system operates under a constant x_{ref} in steady-state conditions. However, during the startup

process, the state variable references will vary, and the time-dependent x_{ref} will be utilized. From this equation, when $u = u_{ref}$, it leads to:

$$\underbrace{\dot{z}}_{u=u_{ref}} = A\left(u_{ref}\right) z + g\left(\hat{p} - p\right) \tag{11}$$

Moreover, when the switching command $u = \{0, 1\}$, the system can be expressed as:

$$\underbrace{\dot{z}}_{u=\{0,1\}} = f\left(z, u\right) + g\left(\hat{p} - p\right) \tag{12}$$

where

$$f(z, u) = A(u)z + A(u)x_{\text{ref}} + B(u) - A(u_{\text{ref}})x_{\text{ref}} - B(u_{\text{ref}})$$

B. ESTIMATOR

A nonlinear estimator comprising the following two equations is proposed to estimate the value of the vector $\hat{p}$, which consists of voltage source V_T and current source I_P:

$$\dot{\hat{z}} = f(z, u) - K_1(\hat{z} - z) \tag{13}$$

$$\dot{\hat{p}} = K_p(\dot{\hat{z}} - \dot{z}) + K_2(\hat{z} - z) - \eta(z)(\hat{z} - z) - \chi \cdot z \tag{14}$$

where the errors between the estimated value and the measurement value of the state variables z and loss variables p are defined as:

$$\xi_z = \hat{z} - z \tag{15}$$

$$\xi_p = \hat{p} - p \tag{16}$$

where $K_1 \in \Re^{n\times n}$ is a positive-definite matrix. $K_2 \in \Re^{n\times m}$, $K_P \in \Re^{n\times m}$, $\eta \in \Re^{n\times m}$, and $\chi \in \Re^{n\times m}$.

To realize the estimator as described in (13) and (14), the time derivative of state variable z is typically required, but measurement noise can cause issues as mentioned in references [32], [35]. Due to limited estimator gain, the quick estimation of unknown parameters can be difficult, leading to overshoot inductor current and a large output voltage drop. In this paper, a change of variable method is proposed to circumvent the need for measuring the signal derivative.

Using (12) and (13), one can find the differential equation of ξ_z:

$$\dot{\xi}_z = \dot{\hat{z}} - \dot{z} = -K_1\xi_z - g(z) \cdot \xi_p \tag{17}$$

Suppose that the variation of p is very slow compared to the state variable, then:

$$\dot{p} = 0 \tag{18}$$

We can find the differential equation of the error ξ_p using (14) and (18) as follows:

$$\dot{\xi}_p = K_p(\dot{\hat{z}} - \dot{z}) + K_2(\hat{z} - z) - \eta(z)(\hat{z} - z) - \chi \cdot z \tag{19}$$

The integration of (19), which is ξ_p with the initial condition $\xi_p = 0$, is used to implement (17). Then, we replace $\dot{\xi}_z$ obtained from (17) in (19) and (14) to calculate $\hat{p}$. The block diagram of this estimator will be provided in Section II-E.

C. SWITCHING COMMAND AND STABILITY ANALYSIS

A Lyapunov stability analysis is employed to demonstrate the exponential stability of the proposed estimator. To do this, a Lyapunov function candidate is chosen and expressed in (20).

$$V = \frac{1}{2}\left(z^T P z + \xi_z^T \xi_z + \xi_p^T \xi_p\right)) \tag{20}$$

Note that the matrix P in the Lyapunov function candidate expressed in (20) is a symmetric positive definite matrix that satisfies the Lyapunov equation, where $A(u_{ref})$ should be the Hurwitz matrix and Q_1 is a symmetric positive definite matrix.

$$A(u_{ref})^T P + PA(u_{ref}) = -Q_1 \tag{21}$$

The switching command is given by a control law, which is defined to control the system as:

$$u(z) = \arg\min_{u\in\{0,1\}} \dot{V} \tag{22}$$

which is a global stability feedback for system (12). Indeed, the derivative of V along the trajectories of (12) yields:

$$\dot{V}(z) = z^T(A(u)^T P + PA(u))z + k = uf_1(z) + (1-u)f_2(z) + k \tag{23}$$

where

$$\begin{aligned} k &= z^T Pg\xi_p + \xi_z^T(-g\xi_p - K_1\xi_z) \\ &\quad + \xi_p^T\begin{bmatrix} K_p(-g\xi_p - K_1\xi_z) + K_2\xi_z - \eta(z)(\hat{z} - z) \\ -\chi \cdot z \end{bmatrix} \\ f_1(z) &= z^T P(A_1 z + A_1 x_{ref} + B_1 - A_1 u_{ref} x_{ref} - B_1 u_{ref}) \end{aligned} \tag{24}$$

and

$$\begin{aligned} f_2(z) = z^T P\Big(&A_2 z + A_2 x_{ref} + B_2 \\ &- A_2(1 - u_{ref})x_{ref} - B_2(1 - u_{ref})\Big) \end{aligned} \tag{25}$$

when $u = u_{ref}$, (23) becomes:

$$\begin{aligned} \dot{V} = u = z^T\Big(A(u_{ref})^T P + PA(u_{ref})\Big)z \\ + z^T Pg\xi_p + \xi_z^T(-g\xi_p - K_1\xi_z) \\ + \xi_p^T\left[K_p(-g\xi_p - K_1\xi_z) + K_2\xi_z - \eta\xi_z - \chi \cdot z\right] \end{aligned} \tag{26}$$

To ensure that the system is exponentially stable, we propose that:

$$\chi = g^T P \tag{27}$$

$$\eta = -g^T \tag{28}$$

$$K_2 = K_p K_1 \tag{29}$$

$$K_1 > 0 \tag{30}$$

$$K_p g = Q_2 > 0 \tag{31}$$

where $Q_2 \in \Re^{m\times m}$ is a positive-definite matrix. Note that because g is not a square matrix,K_p is calculated using the pseudo-inverse of g [36]. With the conditions (27)-(31), when $u = u_{ref}$, equation (26) becomes:

$$\dot{V}(z) = -z^T Q_1 z - \xi_z{}^T K_1 \xi_z - \xi_p{}^T K_p g \xi_p < 0 \tag{32}$$

Equation (32) is strictly negative when $z \neq 0$, $\xi_z \neq 0$, and $\xi_p \neq 0$ because $Q_1 > 0$, $K_1 > 0$, and $K_p g > 0$.

Observe that for $u = u_{ref}$ and with (32), equation (23) becomes:

$$\begin{aligned} &uf_1(z) + (1-u)f_2(z) + k \\ &\quad = -z^T Qz + \xi_p^T(-K_p g)\xi_p - \xi_z^T K_1 \xi_z < 0 \end{aligned} \tag{33}$$

which implies by linearity that

$$\min_{u\in\{0,1\}} \{f_1(z), f_2(z)\} \leq \quad -z^T Q_1 z - \xi_z^T K_1 \xi_z - \xi_p^T K_p g \xi_p < 0 \tag{34}$$

Thus, there always exists a subscript $k \in \{1, 2\}$ such that

$$f_k(z) \leq -z^T Q_1 z - \xi_z{}^T K_1 \xi_z - \xi_p{}^T K_p g \xi_p \tag{35}$$

D. CALCULATION OF P

In [30], the Lyapunov equation shown in (21) is solved to obtain the matrix P using the given symmetric positive definite matrix Q_1 and Hurwitz matrix $A(u_{ref})$, which depends on the operation point u_{ref}. As a result, the matrix P is not constant and changes when the operating point changes. In practice, the matrix P can be calculated online by solving (21) with the Lyap solver in MATLAB, or it can be pre-calculated and stored in a lookup table for each operating point. However, embedding this approach in the practical controller can be challenging. On the other hand, by considering (7)

$$A(u_{ref}) = u_{ref}A_1 + (1-u_{ref})A_2 \tag{36}$$

where $u_{ref} \in 0, 1$, and assuming that A_1 and A_2 are Hurwitz matrices and$P > 0$, then we know that there exist:

$$A_1{}^T P + PA_1 < -Q_1 \tag{37}$$

$$A_2{}^T P + PA_2 < -Q_1 \tag{38}$$

where Q_1 is a symmetric positive definite matrix. Therefore, the first term of (20) becomes:

$$\begin{aligned} &z^T\left(A(u_{\text{ref}})^T P + PA(u_{\text{ref}})\right)z \\ &= u_{\text{ref}} z^T (A_1^T P + PA_1)z + (1-u_{\text{ref}}) z^T (A_2^T P + PA_2)z \\ &\quad < -z^T Q_1 z \end{aligned} \tag{39}$$

As can be observed, the expression $(A_k{}^T P + PA_k)$ with $k \in \{1, 2\}$ does not depend on u_{ref}, and generally, it is independent of the operating point of the system. The solution for the set of equations (37) - (38) is the matrix P, which remains constant for all operating points, making it easy to implement. The matrix P can be pre-calculated offline using the linear matrix inequalities (LMI) solver in MATLAB with only the constant matrices A_1 and A_2 of the system. However, the value of P obtained using LMI may differ significantly from that obtained using (21) for the same value of matrix Q_1 at the nominal load value. Therefore, matrix Q_1 for LMI is adjusted to match the value of P obtained using (21) for the nominal operating point.

E. START-UP PROCESS

Before initiating the system, the power source must supply power to the converter. If the output voltage of the boost converter is equal to the input voltage, the converter's losses can be neglected. At the equilibrium point where $u = u_{ref}$, the state variables are equivalent to the state variable references obtained from the constant output voltage reference V_{oref}., which is generally unchanging. Conversely, during system startup, all state variables transition from the initial equilibrium point to the final equilibrium point. The trajectories of these state variables can be easily computed based on the trajectory of the output voltage. Therefore, the output voltage trajectory should be chosen first, and in this case, we select the response of a second-order system to reduce the inrush current of the output capacitor. The time derivatives of state variable references are required, as shown in equation (10). The block diagram of the proposed controller and observer is depicted in Fig 4. The state variables X_{mes} are sampled at intervals of T_s, and the state variable references X_{ref} are calculated using the desired output voltage V_{oref} and system parameters. Notably, X_{ref} is derived from the output voltage reference, so the time derivative of X_{ref} does not contribute to control noise. An estimator is employed to provide the values of $\hat{z}$ and $\hat{p}$, and the LMI solver in Section *D* determines a constant value of matrix P used to determine the switching command.

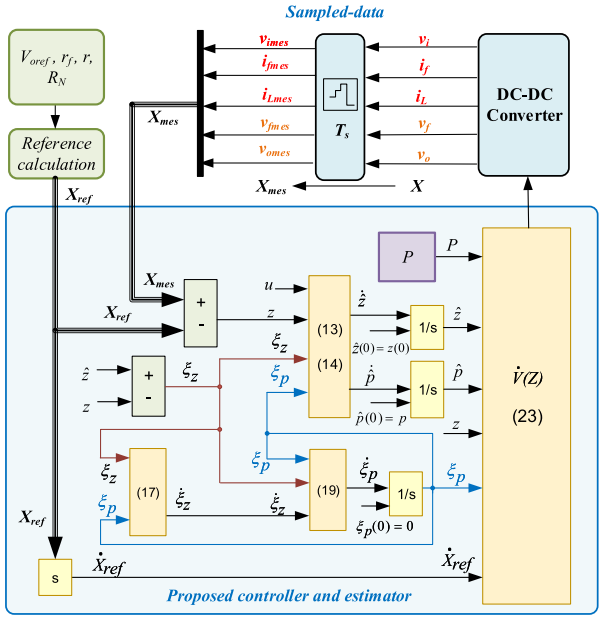

FIGURE 4. Proposed control and estimator diagram.

III. SIMULATION RESULTS

To verify the proposed system, a simulation of the switched model was developed using MATLAB/Simulink. Table 1 shows the parameters of the converter used in the simulation, while the voltage and current sources were included in the model to demonstrate the real effects of the proposed estimator and control algorithm. The currents i_f, i_L and voltages v_f, v_o were sampled in every period $T_s = \frac{1}{f_s}$, and the control and estimator algorithms were executed every T_s. In order to select the appropriate switching command u, which is the output signal of the proposed controller in Fig. 4, several signals had to be sampled.

Matrix Q_1 was chosen, and matrix P was calculated using the system matrices that do not depend on the references, and the LMI solver in MATLAB. For the estimator, an element of matrix Q_2 was selected. The estimated values were then fed into the proposed controller to select the switching command that minimized the candidate Lyapunov function. The control algorithm, which includes the proposed estimator, is illustrated in Fig. 4.

The system and controller parameters are listed in TABLES 1 and 2, respectively.

TABLE 1. System parameters.

Parameter	Quantity	Value
V_i	Input voltage	$63V$
f_s	Sampling frequency	30 kHz
L	Inductance	8.7 mH
C	Output capacitor	875 µF
r	Resistance of inductor	0.2Ω
L_f	Filter inductance	0.55 mH
r_f	Resistance of L_f	0.12Ω
C_f	Filter capacitance	$40\mu F$

TABLE 2. Control parameters.

Parameter	Value
K_1	$\begin{pmatrix} 3000 & 0 & 0 & 0 \\ 0 & 30000 & 0 & 0 \\ 0 & 0 & 1000 & 0 \\ 0 & 0 & 0 & 1500 \end{pmatrix}$
Q_1	$\begin{pmatrix} 1 & 0 & 0 & 0 \\ 0 & 0.1 & 0 & 0 \\ 0 & 0 & 1 & 0 \\ 0 & 0 & 0 & 1.5 \end{pmatrix}$
Q_2	$\begin{pmatrix} 25 & 0 \\ 0 & 25 \end{pmatrix}$
P	$\begin{pmatrix} 0.1937 & 0.0012 & -0.0905 & 0.0016 \\ 0.0012 & 0.0147 & -0.0001 & -0.0001 \\ -0.0905 & -0.0001 & 1.8030 & 0.0257 \\ 0.0016 & -0.0001 & 0.0257 & 0.1855 \end{pmatrix}$
R_N	102Ω
V_{oref}	150 V

A. STARTUP RESPONSE AND STEADY-STATE RESPONSE

The trajectory of the output voltage is selected to reduce an inrush current from the power source and used to derive other references in the controlled system. The simulation results in this section are shown in the following figures. The trajectory of the output voltage is created by feeding the output step voltage reference from 63 V to 150 V through a second-order filter with unity damping factor $\zeta = 1$, and an angular frequency of $\omega_{voref} = 50$ rad/s. In this test, the load resistance is 45 Ω. The responses of the state variables are shown in Fig. 5.

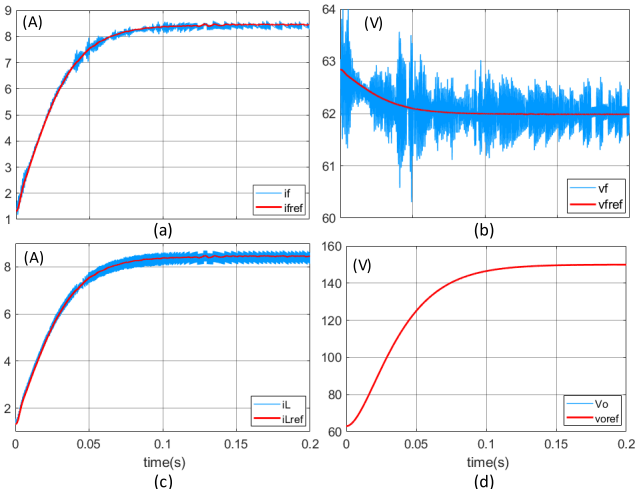

FIGURE 5. Response of (a) input current (i_f) and its reference (i_{fref}) (b) filter capacitor voltage (v_f) and its reference (v_{fref}) (c) inductor current (i_L) and its reference (i_{Lref}) (d) output voltage (v_o) and its reference (v_{oref}). $\omega_{voref} = 50$ rad/s.

In this section, the examination is focused on the dynamics of the state variables with ω_{voref} set to 50 rad/s. The investigation comprises two tests, namely: 1) modifying the output voltage reference and 2) adjusting the resistive load.

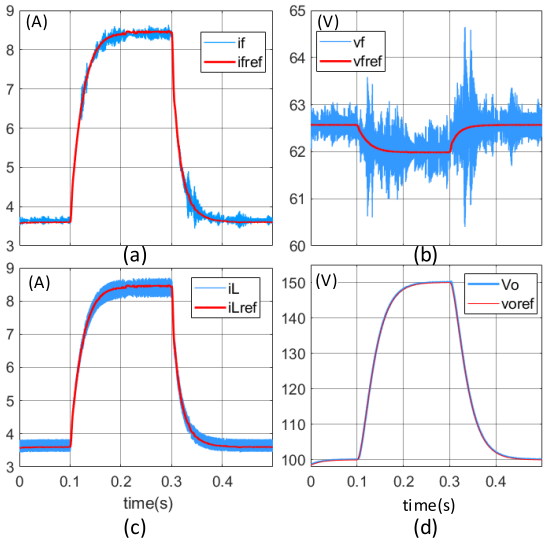

FIGURE 6. Response to output voltage change (a) input current (i_f) and its reference (i_{fref}) (b) filter capacitor voltage (v_f) and its reference (v_{fref}) (c) inductor current (i_L) and its reference (i_{Lref}) (d) output voltage (v_o) and its reference (v_{oref}). $\omega_{voref} = 50$ rad/s.

1) CHANGING OF THE OUTPUT VOLTAGE REFERENCE

Using the same control parameters as in the previous section, the output voltage tracking was evaluated by conducting a test. The test involved altering the output voltage reference from 100 V to 150 V, and the results are illustrated in Fig. 6, depicting the behavior of the state variables. Fig. 6 (a) displays the input current i_f and its reference i_{fref}, while Fig. 6 (b) presents the input filter capacitor voltage v_f and its reference v_f. In both cases, the state variables i_f and v_f are able to track their respective references. Fig. 6 (c) shows the inductor current of the boost converter i_L and its reference i_{Lref}, while Fig. 6 (d) displays the output voltage v_o and its reference v_{oref}.

2) SIMULATION BEHAVIOR OF THE ESTIMATION FOR A LOAD STEP

This test simulates the evolution of the estimated voltage, $\hat{V}_T$, and estimated current, $\hat{I}_P$, during a load step. The output voltage remains constant at 150 V throughout the test, while the load resistance changes from 160Ω to 45Ω at $t = 0.05s$. As shown in Fig. 7, the estimated values of $\hat{V}_T$ and $\hat{I}_P$, respond to the load step and eventually converge to constant values. Prior to $t = 0.05$ s, the load resistance $R = 160$ Ω, which is lower than the nominal load resistance $R_N = 102$ Ω, causing $\hat{I}_P$ to be negative. However, after the load step, with $R = 45$ Ω, $\hat{I}_P$ becomes positive since the load resistance is now below R_N ($R < R_N$).

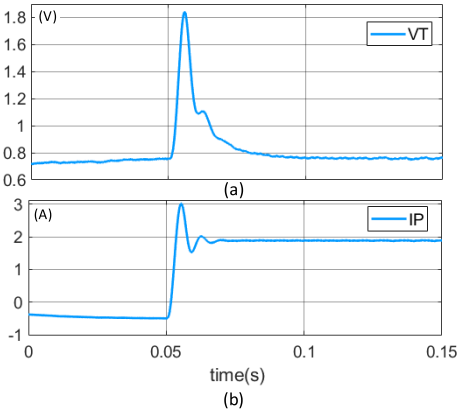

FIGURE 7. Simulation waveforms of $\hat{V}_T$ and $\hat{I}_P$ change of a load resistance from $R = 160$ ohm to $R = 45$ ohm.

3) CHANGING THE RESISTIVE LOAD

In this experiment, the output voltage is regulated at 150 V, while the load resistance is varied from 160Ω to 45Ω. The response of the system's state variables is presented in Figs. 8. As shown, the inductor current of the boost converter increases rapidly from its initial value to the final value, limited by the input voltage and inductance. The output voltage decreases as the current increases, and then returns to its reference level.

To compare our proposed method with a classic control method, we employed a two-loop cascade PI control strategy

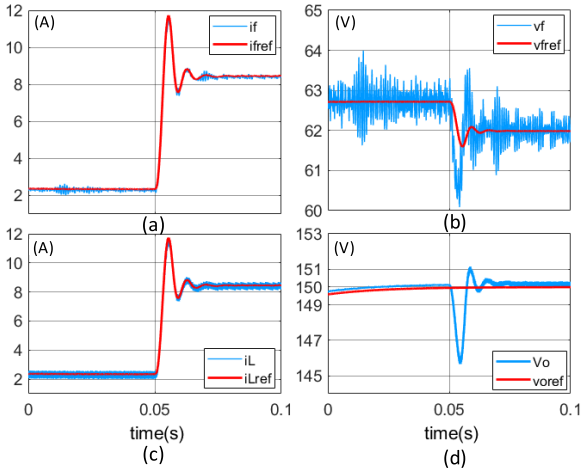

FIGURE 8. Response to load change (a) input current (i_f) and its reference (i_{fref}) (b) filter capacitor voltage (v_f) and its reference (v_{fref}) (c) inductor current (i_L) and its reference (i_{Lref}) (d) output voltage (v_o) and its reference (v_{oref}). $\omega_{voref} = 50$ rad/s.

with a virtual capacitor stabilizer, as described in [20]. The switching frequency $F_{sw} = 30$kHz used in this paper is equal to the sampling frequency f_s. The control strategy achieved a gain margin (GM) greater than 6 dB and a phase margin (PM) of 45 degrees at $\frac{2\pi F_{sw}}{10}$ rad/s and $\frac{2\pi F_{sw}}{300}$ rad/s for the inner current loop and outer voltage loop, respectively.

We observed that the settling time with 2% error of the output voltage using the classic control method was approximately 55 ms, which is higher than the design expectation of 8.8 ms due to the effect of the stabilizer. In contrast, our proposed method achieved a settling time of approximately 6 ms, demonstrating its superior performance.

IV. EXPERIMENTAL RESULTS

To validate the proposed control system, a test bench was set up in the laboratory. The control and estimator algorithms were developed using MATLAB/Simulink and then implemented on dSPACE DS1103, as depicted in Fig. 9. The test bench consisted of various equipment such as a digital oscilloscope, a programmable power supply (63 V/85 A), two variable resistance loads, digital voltmeters, current probes, and a dSPACE unit.

The system utilized an IGBT SKM195GB126D module as a switch and a diode. To measure all necessary signals for the proposed controller, two differential voltage probes and three current probes were employed. This setup ensured accurate measurement of the system's performance and allowed for effective validation of the proposed control system.

The presentation will begin by showcasing the startup and steady-state responses, followed by the transient responses.

A. STARTUP RESPONSE AND STEADY-STATE RESPONSE

The simulation results demonstrate that the output voltage reference is generated by passing the output step voltage reference from 63 V to 150 V through a second-order filter

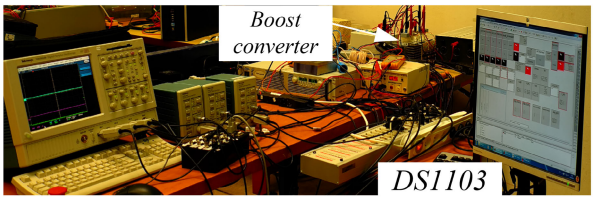

FIGURE 9. Experimental test bench.

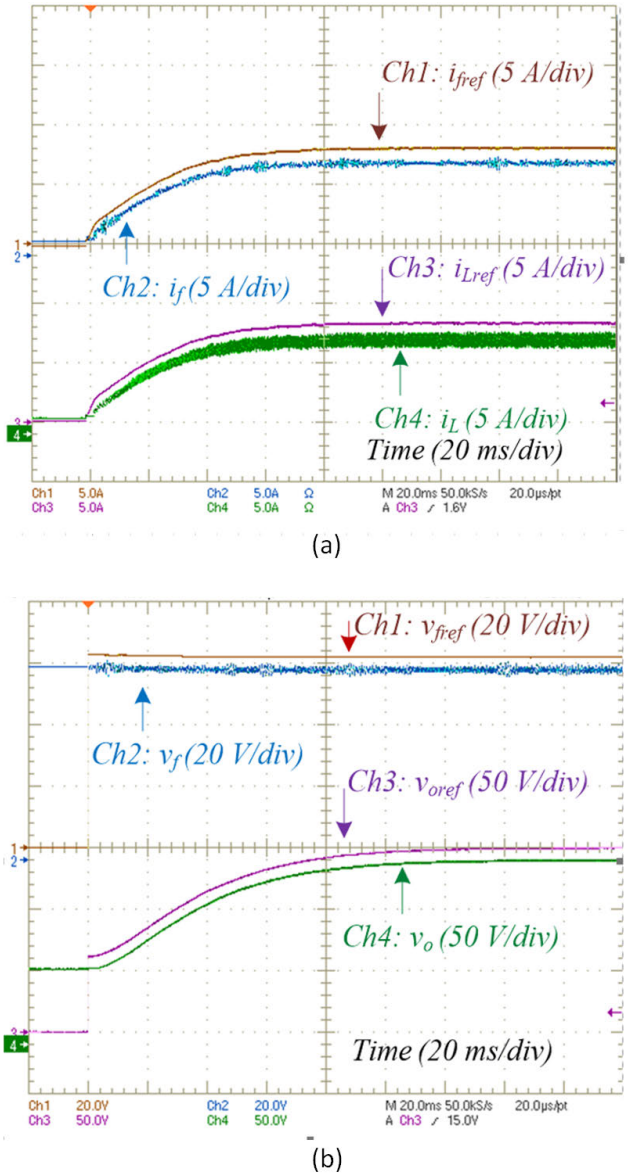

FIGURE 10. (a) Response of the input current and its reference; (b) response of the filter capacitor voltage and its reference.

with unity gain and an angular frequency of $\omega_{voref} = 50$ rad/s. As depicted in Fig. 10, the response of the state variables when the load resistance is 45Ω indicates that the proposed system can be initiated with no input inrush current.

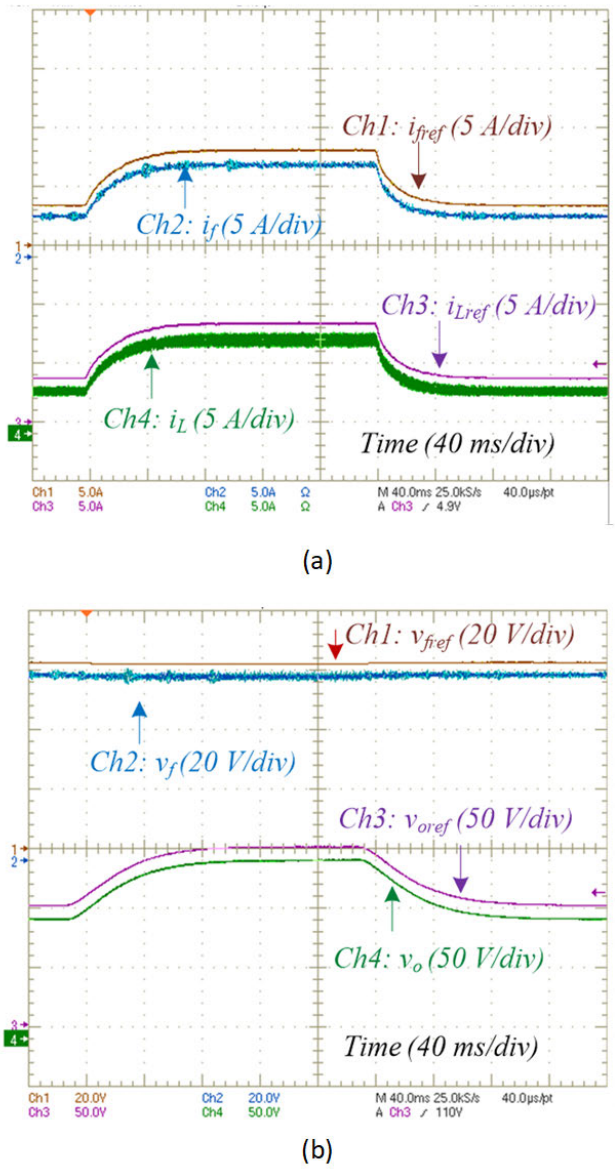

FIGURE 11. (a) Response of the input current and its reference; (b) response of the filter capacitor voltage and its reference.

Furthermore, by selecting the appropriate angular frequency ω_{voref}, the peak current of the input current can be regulated.

B. OUTPUT VOLTAGE TRACKING AND LOAD STEP RESPONSE

In this section, we examine the dynamics of the state variables. Two tests were conducted to achieve this: 1) a change in output voltage and 2) a change in resistive load. The response of the currents i_f, i_L and their references are depicted in Fig. 11 (a) for the first test, while the voltage responses are shown in Fig. 11 (b). All state variables were able to track their reference during both the transient and steady states. In the second test (Fig. 12), the load resistance R was connected to the converter and abruptly reduced from

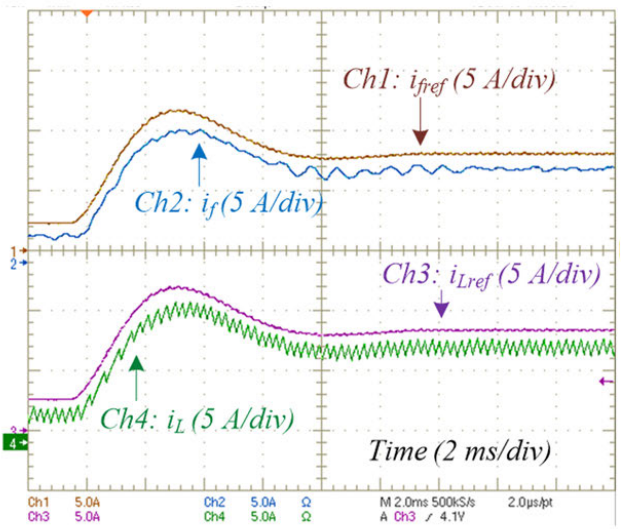

FIGURE 12. Experimental waveforms with the step change of a load resistance from 160 ohms to 45 ohms. (a) Input current and its reference. (b) Response of the filter capacitor voltage and its reference.

160 Ω to 45Ω. The Math function of the oscilloscope was used to determine the output voltage error.

C. EXPERIMENTAL BEHAVIOR OF THE ESTIMATION FOR A LOAD STEP

In this test, we examine the evolution of the voltage $\hat{V}_T$ and current $\hat{I}_P$ during a step load. The output voltage remained constant at 150 V, while the load resistance changed from 160Ω to 45Ω. The estimated values of $\hat{V}_T$ and $\hat{I}_P$ changed initially and then converged to constant values, as demonstrated in Fig.13. During the step load of the output voltage reference, the estimated values of $\hat{V}_T$ and $\hat{I}_P$ converged to their final values. $\hat{I}_P$ was utilized to compensate for the variation in load resistance from the nominal value R_N.

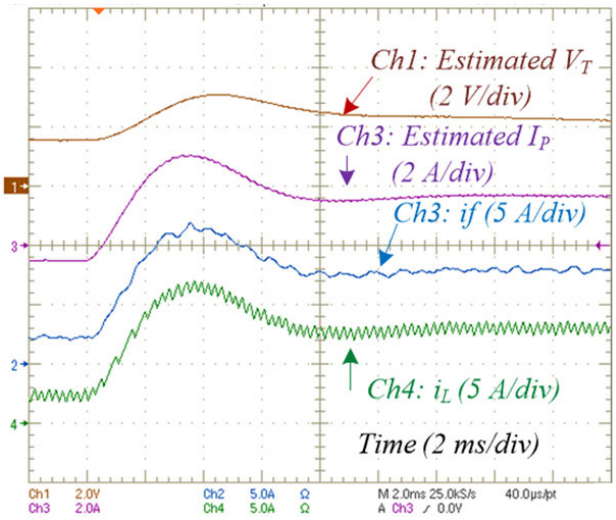

FIGURE 13. Experimental waveforms with the step change of a load resistance from 160 ohms to 45 ohms.

V. CONCLUSION

This paper presents a novel control strategy for a boost converter with an LC input filter by utilizing Lyapunov function. To accurately reflect the real-world scenario, the losses resulting from inductor current and output voltage are estimated online, depending on the operating point. The loss attributed to the output voltage reduces the steady-state error of the control state variables. Furthermore, the proposed loss estimator eliminates the need for a load current sensor. The approach enables the simultaneous control of all converter variables, and the switching command is selected to ensure system stability at all times. The simulation and experimental results demonstrate the effectiveness of the proposed control technique.

REFERENCES

[1] A. A. Saafan, V. Khadkikar, A. Edpuganti, M. S. E. Moursi, and H. H. Zeineldin, "A novel non-isolated four-port converter for flexible DC microgrid operation," *IEEE Trans. Ind. Electron.*, vol. 71, no. 2, pp. 1653–1664, Feb. 2024.

[2] Y. Huang, S. Lin, and H. Mo, "Three level bidirectional DC/DC intelligent control technology for photovoltaic charging station of electric vehicle combined with SVPWM algorithm," *IEEE Access*, vol. 11, pp. 109367–109378, 2023.

[3] M. Yang, Y. Weng, H. Li, J. Lin, X. Yan, and T. Jin, "A novel three-winding coupled inductor-based high-gain DC–DC converter with low switch stress and continuous input current," *IEEE Trans. Power Electron.*, vol. 38, no. 12, pp. 15781–15791, Dec. 2023.

[4] P. Luo, T.-J. Liang, K.-H. Chen, S.-M. Chen, and J.-F. Chen, "Syntheses of three-port DC–DC converters," *IEEE Trans. Power Electron.*, vol. 38, no. 12, pp. 16196–16207, Dec. 2023.

[5] R. Du, V. Samavatian, M. Samavatian, T. Gono, and M. Jasiński, "Development of a high-gain step-up DC/DC power converter with magnetic coupling for low-voltage renewable energy," *IEEE Access*, vol. 11, pp. 90038–90051, 2023.

[6] X. Li, M. Wang, W. Jiang, C. Dong, Z. Xu, and X. Wu, "Towards large-signal stabilization of interleaved floating multilevel boost converter enabled high-power DC microgrids supplying constant power loads," *IEEE Trans. Ind. Electron.*, vol. 71, no. 1, pp. 857–869, Jan. 2024.

[7] F. Guo, Z. Ma, F. Diao, Y. Zhao, and P. Wheeler, "Hybrid virtual coordinate-driven CBPWM strategy of three-level T-type NPC converters for electric aircraft propulsion applications," *IEEE Trans. Ind. Electron.*, vol. 71, no. 3, pp. 2309–2319, Mar. 2024.

[8] Z. Cao, H. Wen, Q. Bu, H. Shi, P. Xu, Y. Yang, and Y. Du, "Constant power load stabilization with fast transient boundary control for DAB converters-based electric drive systems," *IEEE Trans. Ind. Electron.*, vol. 71, no. 2, pp. 1863–1874, Feb. 2024.

[9] S. Li, X. Yu, Y. Yuan, S. Lu, and T. Li, "A novel high-voltage power supply with MHz WPT techniques: Achieving high-efficiency, high-isolation, and high-power-density," *IEEE Trans. Power Electron.*, vol. 38, no. 12, pp. 14794–14805, Dec. 2023.

[10] Y. Cao, Y. Bai, V. Mitrovic, B. Fan, D. Dong, R. Burgos, D. Boroyevich, R. K. Moorthy, and M. Chinthavali, "A three-level buck-boost converter with planar coupled inductor and common-mode noise suppression," *IEEE Trans. Power Electron.*, vol. 38, no. 9, pp. 10483–10500, Sep. 2023.

[11] N. O. Sokal, "System oscillations from negative input resistance at power input port of switching-mode regulator, amplifier, DC/DC converter, or DC/DC inverter," in *Proc. IEEE Power Electron. Spec. Conf.*, Jun. 1973, pp. 138–140.

[12] R. D. Middlebrook, "Input filter consideration in design and application of switching regulators," in *Proc. IEEE Ind. Appl. Soc. Annu. Meeting*, Jan. 1976, pp. 366–382.

[13] L.-M. Saublet, R. Gavagsaz-Ghoachani, J.-P. Martin, B. Nahid-Mobarakeh, and S. Pierfederici, "Asymptotic stability analysis of the limit cycle of a cascaded DC–DC converter using sampled discrete-time modeling," *IEEE Trans. Ind. Electron.*, vol. 63, no. 4, pp. 2477–2487, Apr. 2016.

[14] A. Suyapan, K. Areerak, S. Bozhko, S. S. Yeoh, and K. Areerak, "Adaptive stabilization of a permanent magnet synchronous generator-based DC electrical power system in more electric aircraft," *IEEE Trans. Transport. Electrific.*, vol. 7, no. 4, pp. 2965–2975, Dec. 2021.

[15] R. Gavagsaz-Ghoachani, J.-P. Martin, S. Pierfederici, B. Nahid-Mobarakeh, and B. Davat, "DC power networks with very low capacitances for transportation systems: Dynamic behavior analysis," *IEEE Trans. Power Electron.*, vol. 28, no. 12, pp. 5865–5877, Dec. 2013.

[16] R. Shen and H. S. Chung, "On the use of nonlinear inductor to enhance the stability of DC distribution networks," *IEEE Trans. Power Electron.*, vol. 37, no. 7, pp. 8582–8595, Jul. 2022.

[17] P. Magne, D. Marx, B. Nahid-Mobarakeh, and S. Pierfederici, "Large signal stabilization of a DC-link supplying a constant power load using a virtual capacitor: Impact on the domain of attraction," *IEEE Trans. Ind. Appl.*, vol. 48, no. 3, pp. 878–887, Jun. 2012.

[18] M. Karbalaye Zadeh, R. Gavagsaz-Ghoachani, S. Pierfederici, B. Nahid-Mobarakeh, and M. Molinas, "Stability analysis and dynamic performance evaluation of a power electronics-based DC distribution system with active stabilizer," *IEEE J. Emerg. Sel. Topics Power Electron.*, vol. 4, no. 1, pp. 93–102, Mar. 2016.

[19] M. K. Zadeh, R. Gavagsaz-Ghoachani, J.-P. Martin, B. Nahid-Mobarakeh, S. Pierfederici, and M. Molinas, "Discrete-time modeling, stability analysis, and active stabilization of DC distribution systems with multiple constant power loads," *IEEE Trans. Ind. Appl.*, vol. 52, no. 6, pp. 4888–4898, Nov. 2016.

[20] L.-M. Saublet, R. Gavagsaz-Ghoachani, J.-P. Martin, B. Nahid-Mobarakeh, and S. Pierfederici, "Bifurcation analysis and stabilization of DC power systems for electrified transportation systems," *IEEE Trans. Transport. Electrific.*, vol. 2, no. 1, pp. 86–95, Mar. 2016.

[21] Y. Huangfu, S. Pang, B. Nahid-Mobarakeh, L. Guo, A. K. Rathore, and F. Gao, "Stability analysis and active stabilization of on-board DC power converter system with input filter," *IEEE Trans. Ind. Electron.*, vol. 65, no. 1, pp. 790–799, Jan. 2018.

[22] M. Wu and D. D. Lu, "A novel stabilization method of LC input filter with constant power loads without load performance compromise in DC microgrids," *IEEE Trans. Ind. Electron.*, vol. 62, no. 7, pp. 4552–4562, Jul. 2015.

[23] H.-J. Kim, S.-W. Kang, G.-S. Seo, P. Jang, and B.-H. Cho, "Large-signal stability analysis of DC power system with shunt active damper," *IEEE Trans. Ind. Electron.*, vol. 63, no. 10, pp. 6270–6280, Oct. 2016.

[24] X. Zhang, Q.-C. Zhong, and W.-L. Ming, "A virtual RLC damper to stabilize DC/DC converters having an LC input filter while improving the filter performance," *IEEE Trans. Power Electron.*, vol. 31, no. 12, pp. 8017–8023, Dec. 2016.

[25] A.-B. Awan, S. Pierfederici, B. Nahid-Mobarakeh, and F. Meibody-Tabar, "Active stabilization of a poorly damped input filter supplying a constant power load," in *Proc. IEEE Energy Convers. Congr. Exposit.*, Sep. 2009, pp. 2991–2997.

[26] M. U. Iftikhar, E. Godoy, P. Lefranc, D. Sadarnac, and C. Karimi, "A control strategy to stabilize PWM DC–DC converters with input filters using state-feedback and pole-placement," in *Proc. INTELEC IEEE 30th Int. Telecommun. Energy Conf.*, Sep. 2008, pp. 1–5.

[27] R. Gavagsaz-Ghoachani, M. Phattanasak, J.-P. Martin, S. Pierfederici, B. Nahid-Mobarakeh, and P. Riedinger, "A Lyapunov function for switching command of a DC–DC power converter with an LC input filter," *IEEE Trans. Ind. Appl.*, vol. 53, no. 5, pp. 5041–5050, Sep. 2017.

[28] P. Riedinger and J.-C. Vivalda, "Dynamic output feedback for switched linear systems based on a LQG design," *Automatica*, vol. 54, pp. 235–245, Apr. 2015.

[29] C. Albea, G. Garcia, and L. Zaccarian, "Hybrid dynamic modeling and control of switched affine systems: Application to DC–DC converters," in *Proc. 54th IEEE Conf. Decis. Control (CDC)*, Dec. 2015, pp. 2264–2269.

[30] G. Deaecto, J. Geromel, F. Garcia, and J. Pomilio, "Switched affine systems control design with application to DC–DC converters," *IET Control Theory Appl.*, vol. 4, no. 7, pp. 1201–1210, 2010.

[31] P. Hauroigne, P. Riedinger, and C. Iung, "Switched affine systems using sampled-data controllers: Robust and guaranteed stabilization," *IEEE Trans. Autom. Control*, vol. 56, no. 12, pp. 2929–2935, Dec. 2011.

[32] J. A. Solsona, S. G. Jorge, and C. A. Busada, "Nonlinear control of a buck converter which feeds a constant power load," *IEEE Trans. Power Electron.*, vol. 30, no. 12, pp. 7193–7201, Dec. 2015.

[33] H. Renaudineau, J. Martin, B. Nahid-Mobarakeh, and S. Pierfederici, "DC–DC converters dynamic modeling with state observer-based parameter estimation," *IEEE Trans. Power Electron.*, vol. 30, no. 6, pp. 3356–3363, Jun. 2015.

[34] M. Phattanasak, R. Gavagsaz-Ghoachani, J.-P. Martin, S. Pierfederici, B. Nahid-Mobarakeh, and P. Riedinger, "Improved performance of a control using switching command based on Lyapunov functions of a boost converter with an LC input filter," in *Proc. Int. Conf. Electr. Syst. Aircr., Railway, Ship Propuls. Road Vehicles Int. Transp. Electrific. Conf. (ESARS-ITEC)*, Nov. 2016, pp. 1–6.

[35] Z. Xin, X. Wang, P. C. Loh, and F. Blaabjerg, "Realization of digital differentiator using generalized integrator for power converters," *IEEE Trans. Power Electron.*, vol. 30, no. 12, pp. 6520–6523, Dec. 2015.

[36] A. Ben-Israel and T. Greville, *Generalized Inverses—Theory and Applications*, 2nd ed. New York, NY, USA: Wiley-Interscience, 2000.

ROGHAYEH GAVAGSAZ-GHOACHANI received the M.Sc. degree from Institut National Polytechnique de Lorraine (INPL), Nancy, France, in 2007, and the Ph.D. degree from the University of Lorraine, Vandoeuvre-lès-Nancy, France, in 2012, all in electrical engineering. She is currently an Associate Professor with the Department of Renewable Energies Engineering, Shahid Beheshti University, Tehran, Iran. She is also a Researcher with Groupe de Recherche en Electrotechnique et Electronique de Nancy (GREEN) and Laboratoire d'Energétique et de Mécanique Théorique et Appliquée (LEMTA), University of Lorraine. Her current research interests include the stability study, control of power electronics systems, and renewable energy.

MATHEEPOT PHATTANASAK (Senior Member, IEEE) received the B.Sc. and M.E. degrees in electrical engineering from the King Mongkut's Institute of Technology North Bangkok (KMITNB), Bangkok, Thailand, in 1996 and 2004, respectively, and the Ph.D. degree in electrical engineering from the University of Lorraine, Nancy, Lorraine, France, in 2012. He is currently a Full Professor with the Department of Teacher Training in Electrical Engineering (TE), King Mongkut's University of Technology North Bangkok (KMUTNB), Bangkok. His current research interests include power electronics and their controllers.

EHSAN JAMSHIDPOUR (Senior Member, IEEE) received the M.S. degree in electrical engineering from the Sharif University of Technology, Tehran, Iran, in 2001, and the Ph.D. degree in electrical engineering from the University of Lorraine, Nancy, France, in 2014. From 2003 to 2010, he was an Assistant Professor with the Institute for Energy and Hydro Technology, Kermanshah, Iran. From 2016 to 2020, he was with ECAM Strasbourg Europe as a Senior Lecturer and also with the ICube Laboratory, University of Strasbourg. In September 2020, he joined Ecole Nationale Superieure d'Electricite et de Mecanique (ENSEM), University of Lorraine, where he is currently an Assistant Professor. He is also with the GREEN Laboratory, Nancy. His main research interests include electric motor drives, fault detection and fault-tolerant of power electronic converters, and renewable energy. He is an Associate Editor of IEEE TRANSACTIONS ON TRANSPORTATION ELECTRIFICATION.

WISET SAKSIRI received the B.Sc. and M.E. degrees in electrical engineering from the King Mongkut's Institute of Technology North Bangkok (KMITNB), Bangkok, Thailand, in 1995 and 1999, respectively. He is an Assistant Professor of electrical engineering with the King Mongkut's University of Technology North Bangkok (KMUTNB), Bangkok. His main research interests include electric motor drives, fault diagnosis of power electronic converters, renewable energy, and their controllers.

SERGE PIERFEDERICI received the Engineer degree from Ecole Nationale Supérieure d'Electricité et Mécanique, Nancy, France, in 1994, and the Ph.D. degree from Institut National Polytechnique de Lorraine, Nancy, in 1998, all in electrical engineering. Since 2009, he has been a Full Professor with the University of Lorraine, Nancy. He has authored or coauthored more than 200 articles, which are published in the international peer-reviewed journals. His research interests include the stability study of distributed power systems and modeling and control of power electronic systems. In recent years, his research interests are in the areas of the distributed control of multisources and multicarrier microgrids. He serves on the editorial boards for the international peer-reviewed journals.